ARTICLES

Takens-Bogdanov random walks

E. R. Tracy,* X. Z. Tang,† and C. Kulp‡
Physics Department, College of William & Mary, Williamsburg, Virginia 23187-8795
(Received 11 December 1997)

Takens-Bogdanov bifurcations have linearized dynamics that are nondiagonalizable. The *nonlinear* response of such systems to perturbations is quite distinct from systems with diagonalizable linearizations. While Takens-Bogdanov systems are of central importance in the theory of local codimension-two bifurcations, their physical relevance is unclear because they are topologically fragile. Only those properties that are robust under the breaking of the exact degeneracy required for nondiagonalizability are likely to have any physical significance. In this paper we consider the steady-state noise response of degenerate and nearly degenerate nodes in N dimensions. Escape times are computed for the subcritical case and shown to obey scaling relations that are different from those of normal systems. The scaling behavior at high noise levels can be extracted from the related Fokker-Planck equation and is robust to weak breaking of the exact degeneracy.
[S1063-651X(98)10704-3]

PACS number(s): 05.40.+j, 02.50.Ey

I. INTRODUCTION

In this paper we shall be interested in the noise response of nonlinear systems that, when linearized about a stable fixed point, are either nondiagonalizable or very nearly so (in numerical analysis such linear systems are called *ill conditioned*). In the bifurcation literature these systems are said to be of ''Takens-Bogdanov'' type [1,2]. Such bifurcations are known to occur in low-dimensional models of bounded shear flows near the laminar or turbulent transition [4–8]. They also arise in aeroelastic flutter models [9], and stall models for turbines [10]. For a discussion of the related degenerate Hopf bifurcation, the reader is referred to Refs. [11,12].

As a simple example, consider the two-dimensional (2D) linear flow associated with a stable degenerate node:

$$\begin{pmatrix} \dot{x}_1 \\ \dot{x}_2 \end{pmatrix} = \begin{pmatrix} -\epsilon & 1 \\ 0 & -\epsilon \end{pmatrix} \begin{pmatrix} x_1 \\ x_2 \end{pmatrix}. \tag{1}$$

The threshold for linear instability is $\epsilon=0$, where the flow has a pure shear character and the 2×2 matrix is nondiagonalizable. If one is interested in the bifurcation characteristics of this system when nonlinear terms are added, then one is led to the theory of normal forms. It is remarkable that, although the theory of normal forms was introduced by Poincaré and Birkhoff, the normal form analysis for Eq. (1) was not carried out until the 1970s [1,2] (see Chapter 7 of the most recent edition of [3] for a very complete discussion).

In applications, low-dimensional models are often derived via Galerkin projection, or some other reduction scheme, onto the center manifold of the much larger—often infinite-dimensional—system [3,9]. The connection between the bifurcation behavior of the low-dimensional model and the original high-dimensional dynamical system must be carefully established, especially when the low-dimensional system is nearly degenerate and, hence, structurally fragile in a topological sense. For example, if we nonlinearly perturb the dynamical system (1) about the neutral threshold $\epsilon=0$ the degenerate node can convert into a nondegenerate node, a saddle, a stable or unstable spiral. The interested reader is referred to the unfolding diagram on p. 367 of [3], which shows the variety of behaviors that can occur. Such an unfolding diagram reveals how the degenerate topology is modified as parameters are varied. It is possible, however, that a fragile topological structure can be accompanied by other physically relevant aspects of the dynamics that behave in a smooth and well-behaved manner. What is meant by ''physically relevant'' depends upon the problem of interest.

Here we examine how Takens-Bogdanov systems respond to noise driving, using the degenerate node of Eq. (3) as our model. This noise might represent couplings to degrees of freedom that have been projected out by the reduction procedure, or the influence of the environment. We focus primarily on the linearly stable regime $\epsilon>0$ and the subcritical case, where the addition of nonlinearity introduces a basin boundary in the vicinity of the node. This implies that, although the system is linearly stable, it is *nonlinearly* unstable to perturbations of sufficient size to cross the basin boundary. Noise perturbations can lead the system to escape the vicinity of the node, and we are particularly interested in how the average escape time, τ, depends on various parameters, such as the noise level σ_η, the bifurcation parameter ϵ, and the dimensionality of the system, N.

*Electronic address: tracy@physics.wm.edu
†Present address: Department of Applied Physics, Columbia University, New York, NY 10027. Electronic address: tang@chaos.ap.columbia.edu
‡Permanent address: Physics Department, Western Maryland College, 2 College Hill, Westminster, MD 21157.

Although the linearly stable case is the focus of this paper, some of our results are similar to those for the linearly *unstable* case, in particular the scaling behavior of the escape time τ at high noise levels. This is because at high noise levels the system does not ''see'' the small stable basin surrounding the fixed point, even if it exists, and is instead guided by the larger-scale structure of the phase space flow in the vicinity. We mention in particular that for chaotic systems with homoclinic tangencies, Sauer *et al.* [13] also report power law behavior for the *shadowing time*, which is the unstable analog of the escape time τ, discussed below. The escape time scaling for the linearly unstable case is considered here, briefly, in Sec. V.

Our results show that the noise response of degenerate, and nearly degenerate, nodes is quite different from the normal situation where the linearized dynamics is far from degeneracy. In addition, the statistical behavior of the system varies smoothly in the vicinity of degeneracy. In this sense, the structural instability of the phase space topology is less important than one might imagine because the noise ''frees'' the system from having to slavishly follow the underlying topology. The dynamics is then guided by coarser features of the phase space flow, which are relatively robust.

Random walks with degenerate linear terms appear not to have received much attention [14]. Aside from the work of Farrell *et al.* [5] on the stochastically driven *linearized* Navier-Stokes equations we are not aware of any previous work in the literature. (We mention, however, the recent work of Sauer *et al.* [13], and Jaeger and Kantz [15], which deal with the effect of noise on nonhyperbolic chaotic systems. These, however, are globally unstable while we are interested in the effect of noise on a stable fixed point.)

Here we consider simplified discrete-time *nonlinear* models in an attempt to gain general insight, though the form of Eq. (4) was suggested by some low-dimensional models of shear *flows* discussed in [7]. Maps have the distinct advantage of allowing one to generate large ensembles and look at very long-time behavior.

The outline of the paper is as follows: in Sec. II the noise-free case is discussed. The steady-state noise response is discussed in Sec. III and numerical results for the exactly degenerate case presented. The results are easily understood in terms of a few simple scaling relations discussed in Sec. IV. In Sec. V the effects of breaking the exact degeneracy are examined. In this section the linearly *unstable* case is also briefly considered. We end with a short summary in Sec. VI.

II. BASIC THEORY: NOISE-FREE DYNAMICS

Consider a nonlinear discrete-time dynamical system in N dimensions:

$$x_j(m+1)=F_j(x(m);p), \quad m=0,1,2\ldots, \tag{2}$$

where $x,F\in\mathbb{R}^N$, F is a smooth vector function of x, and p is a bifurcation control parameter. Suppose F has a fixed point $x_*(p)$, which we take to be the origin. Taylor expanding to first order in x gives (repeated indices are summed):

$$x_j(m+1)=A_{jk}x_k(m), \quad j=1,2,\ldots,N, \tag{3}$$

with $A\equiv\nabla F|_{x=0}$. We take A to be of Jordan block form:

$$A\equiv\begin{pmatrix} \lambda & 1 & \ldots & 0 \\ 0 & \lambda & 1 & \vdots \\ & & \cdot & \cdot \\ \vdots & & \cdot & 1 \\ 0 & \ldots & & \lambda \end{pmatrix}. \tag{4}$$

Aside from the diagonal immediately above the main diagonal, filled here with 1's, all other off-diagonal terms indicated by dots are zero. The eigenvalue λ is assumed real and $\lambda^2<1$, hence the fixed point is either a degenerate node ($\lambda>0$), or a degenerate flip node ($\lambda<0$). The exact degeneracy of the eigenvalues and the uniformity of the off-diagonal coupling makes the analysis tractable. The resulting scaling relations were then tested numerically and found to be robust if the degeneracy and uniformity are only approximate. The treatment of more general upper triangular matrices will be discussed elsewhere. It is easy to verify that the above matrix has only one eigenvector (it lies in the x_1 direction), and is therefore not diagonalizable. Neutral stability occurs when $\lambda=1$.

In previous work [16] we studied the impulse response of the degenerate node using a normal form analysis, in Takens and Bogdanov form [1–3]. It is possible to show that near threshold ($\lambda\approx1$) the dominant nonlinear term is of the form

$$x_j(m+1)=A_{jk}x_k(m)+bx_1^n(m)\,\delta_{jN}. \tag{5}$$

As discussed in [3], Takens arrived at this result (for the $N=n=2$ case) using the technique of *topological blowup*, while our work of [16] used asymptotic balance arguments. If this dominant nonlinear term is absent, then one must systematically search for the subdominant nonlinearities, a rich topic in itself and well outside the range of the present paper. For the purposes of this paper, we will set $b=1$ and assume that the dominant nonlinearity is quadratic ($n=2$). The dimensionality N is arbitrary.

Now write $\lambda\equiv1-\epsilon$ and use ϵ as the bifurcation control parameter. Since the nonlinear coupling constant is positive, it is easy to show that Eq. (5) now has a second fixed point at

$$x_{1s}=\epsilon^N; \quad x_{2s}=\epsilon x_{1s}; \quad x_{3s}=\epsilon x_{2s}; \quad \ldots. \tag{6}$$

Linearizing about this second fixed point shows that it is of saddle type. [More precisely, the eigenvalues of the linearized matrix can have imaginary parts of $O(\epsilon)$, but one of them is always real and greater than one and its unstable manifold connects back to the node, forming the ''saddle-sink connection''.]

The stable manifold of the saddle forms the basin boundary. The degeneracy of the node causes the saddle to also be nearly degenerate, which forces the basin boundary to lie close to the node. The distance of closest approach σ_c is the threshold for finite amplitude impulsive perturbations to drive the system unstable. This is summarized in Fig. 1. The shape of the triangle OAS is determined by the transient *linear* amplification factor, which can be estimated as follows [16]: at the initial time, $m=0$, give the system a kick in the x_N direction of magnitude δ_0, hence $x_0=(0,0,\ldots,\delta_0)^T$ where T denotes transpose. After m time

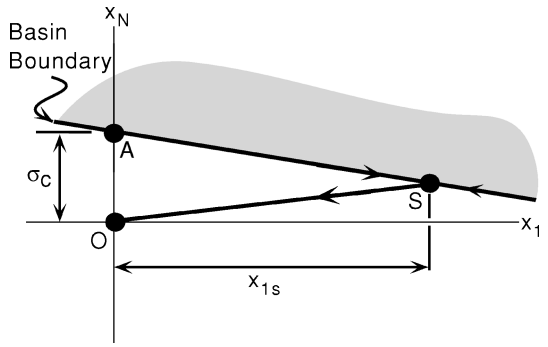

FIG. 1. The geometry of the basin boundary in the neighborhood of the saddle-node connection.

steps this initial condition moves to $x(m)=A^m x_0$, therefore $x_1(m)=[A^m]_{1N}\delta_0$. Some algebra shows that

$$[A^m]_{1N}=\binom{m}{N-1}\lambda^{m+1-N}. \tag{7}$$

Taking $\lambda=1-\epsilon\uparrow 1$, rewriting $m=t/\epsilon$ with $t\sim O(1)$, and using $(1-\epsilon)^{t/\epsilon}\sim e^{-t}$ as $\epsilon\downarrow 0$ leads to

$$|x_1|_{\max}\sim\delta_0\epsilon^{1-N}. \tag{8}$$

(Note that this is also valid for $N=1$.) The maximum occurs on a time scale of $\sim N/\epsilon$. The ratio $|x_1|_{\max}/\delta_0$ is of the same order as x_{1s}/σ_c, which leads to an estimate of σ_c:

$$\sigma_c\sim\epsilon^{2N-1}. \tag{9}$$

This scaling behavior was tested numerically in [16] and found to hold with high precision even if the degeneracy was weakly broken. This summarizes the impulse response of the undriven system.

III. THE STEADY-STATE NOISE RESPONSE

Now consider the steady-state noise response. That is, Eq. (5) is modified by adding a noise driver:

$$x_j(m+1)=A_{jk}x_k(m)+x_1^2(m)\,\delta_{jN}+\eta_j(m) \tag{10}$$

with $\eta\in\mathbb{R}^N$. The noise is assumed to be Gaussian white with correlation tensor $\langle\eta(n)\,\eta^T(m)\rangle=\sigma_\eta^2\delta_{mn}I$, and I the $N\times N$ identity matrix. The use of a more general form of white-noise correlation tensor merely complicates the algebra without introducing substantially new effects. However, it is known that colored noise can substantially affect fluctuation behavior [17].

As a function of the noise level, σ_η, there are three distinct regimes: (1) high noise, $\sigma_\eta\gg\sigma_c$, where the random walker escapes on a time scale $\tau\sim\sigma_\eta^{-\nu_N}$. Here ν_N depends only on the dimensionality of the system and is determined by the escape behavior at threshold ($\epsilon=0$). In Sec. IV it is shown that $\nu_N=2/(4N-1)$ by appealing to the scaling behavior of the *continuous-time* Fokker-Planck equation. (2) Moderate noise, where $\sigma_\eta\approx\sigma_c$, the random walker undergoes transient linear amplification, which brings it into the vicinity of the saddle on a time scale of $O(N/\epsilon)$ where it can escape. And (3) low noise, $\sigma_\eta\ll\sigma_c$, where the random walker is confined to the saddle-sink connection and the escape time quickly grows without bound as the noise level is reduced below a critical value, $\sigma_{\min}$. An estimate is developed in Sec. IV for $\sigma_{\min}$.

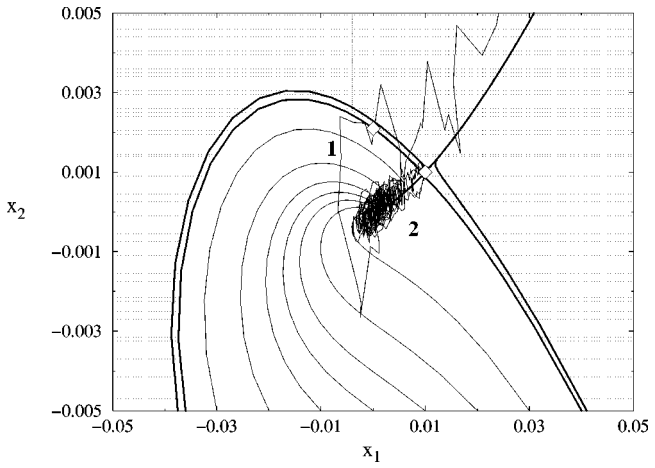

FIG. 2. Typical random walk behavior for a 2D map.

Figure 2 illustrates the moderate- and low-noise regimes for the 2D case with bifurcation parameter $\epsilon=0.1$. (The high-noise walker would leave the figure in a single time step.) The unshaded region consists of those points which, with no noise present, eventually asymptote to the node at the origin. The smooth curves starting at the bottom of the figure represent orbits of the undriven dynamics, with the four orbits lying in close proximity to the basin boundary drawn in heavier weight to emphasize the stable and unstable manifolds of the saddle point. Note that the x_2 scale and x_1 scale differ by a factor of ϵ. The saddle point [at $(x_{1s},x_{2s})=(\epsilon^N,\epsilon^{N+1})$] and the point of closest approach of the basin boundary to the node [at $(x_{1c},x_{2c})=(0,\sigma_c)=(0,\epsilon^{2N-1})$] are indicated by the open diamonds.

The orbit marked 1 is a moderate-noise random walk with $\sigma_\eta=\sigma_c$. Notice that it leaves the basin in the vicinity of (x_{1c},x_{2c}), having been ''urged'' in that direction by the deterministic part of the dynamics. It leaves the basin in a time of $O(2/\epsilon)$, then follows the unstable manifold of the saddle out to large amplitudes.

The orbit marked 2 is a low-noise orbit with $\sigma_\eta=\sigma_{\min}=(\sqrt{2}/3)\epsilon^{2N-1/2}$, i.e., the noise threshold where escape shuts off (estimated in Sec. IV). Notice that the random walk is confined to the saddle-sink connection. The walker has not escaped after 10^4 iterations, though it will eventually.

Figures 3 and 4 show the averaged results of a large number of numerical runs. For each value of ϵ and σ_η 10 000 realizations were generated. All realizations started at the origin and escape was defined as the particle reaching $|x|\approx 1$. (Recall that the unstable manifold of the saddle lies nearly along the positive x axis and is the escape channel.)

Figure 3 shows the effect of varying ϵ with the dimensionality held fixed at $N=4$. Notice that all curves asymptote to the same scaling behavior at high noise, and that this scaling behavior is given by the noise response at threshold ($\epsilon=0$). This is because at high noise the random walker does not ''see'' the fact that there is a basin present (which vanishes at the threshold for linear instability).

For $\epsilon=0.01$, the vertical lines mark the magnitudes of $x_{1s}=\epsilon^N=\epsilon^4$, $\sigma_c=\epsilon^{2N-1}=\epsilon^7$, and $\sigma_{\min}=\epsilon^{2N-1/2}\sqrt{2}/3$

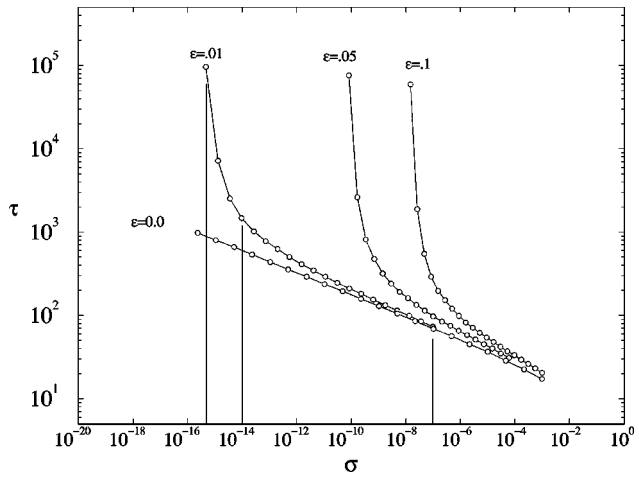

FIG. 3. The mean escape time in four dimensions as a function of the noise amplitude, plotted for four different values of the bifurcation parameter. Data points are connected by a line for clarity. Notice that all curves asymptote to the $\epsilon=0$ scaling at high noise. The vertical lines connecting to the $\epsilon=0.01$ data are explained in the text.

$=\epsilon^{15/2}\sqrt{2}/3$. (Similar indications are not made on the $\epsilon=0.05$, and 0.1 data in order to keep the graph from becoming too busy.) The maximum noise value used in each case is one decade larger than x_{1s} in order to emphasize the smooth behavior of the escape time in the vicinity of $\sigma_\eta \sim x_{1s}$. Not shown are numerical calculations that show that the scaling behavior $\tau \sim \sigma_\eta^{-\nu_N}$ continues up to $\sigma_\eta \sim 1$, where the escape time becomes of order unity and, hence, bottoms out for the discrete-time map we consider. (For these high noise runs we defined escape to be $|x| \approx 10^4$ to avoid introducing boundary effects in the scaling.) As the noise level is reduced, the high-noise scaling breaks down when $\sigma_\eta \sim \sigma_c$. As σ_η drops below σ_c the escape time increases rapidly and effectively becomes unbounded for $\sigma_\eta \ll \sigma_{\min}$.

Figure 4 shows the effect of varying the dimension N for a fixed bifurcation parameter ϵ. The curves with open symbols were generated with bifurcation parameter fixed at ϵ

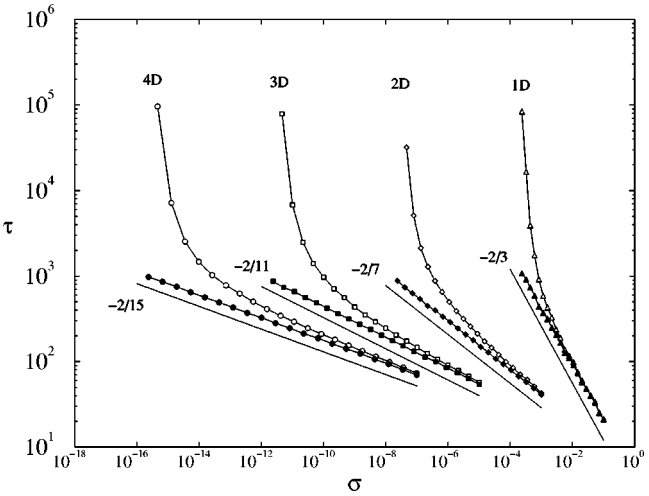

FIG. 4. The mean escape time vs the noise amplitude in $N=1$, 2, 3, and 4 dimensions. For each N, the escape time was computed for both $\epsilon=0.01$ and 0. See the text for a full explanation.

$=0.01$, while those with closed symbols were generated with $\epsilon=0$. The data were generated as in Fig. 3. As in that figure, each curve was generated with a maximum noise value one order of magnitude greater than $x_{1s}=\epsilon^N=10^{-2N}$. Notice that the threshold ($\epsilon=0$) scaling behaviors depend strongly on N.

The solid lines lying in the vicinity of each data set obey the scaling law

$$\tau \sim \sigma_\eta^{-\nu_N} \tag{11}$$

with $\nu_N \equiv 2/(4N-1)$. The values of $-\nu_N$ are indicated beside each curve. The normalization constant [absent from Eq. (11)] was chosen by hand to make the curves easy to compare. The normalizations used were 3, 4, 5, and 6 for $N=1$, 2, 3, and 4, respectively.

IV. ESTIMATES OF $\sigma_{\min}$ AND ν_N

We now turn to the estimates of $\sigma_{\min}$, the noise level where escape shuts down, and ν_N, the scaling exponent for the escape time at threshold ($\epsilon=0$) (as well as the high-noise scaling behavior).

The magnitude of $\sigma_{\min}$ can be estimated by considering Fig. 2 once again. At low noise the random walk is confined to the saddle-sink connection. We can use the linear response to noise driving to estimate the rms value of $|x_1|$. If this is substantially less than the distance to the saddle x_{1s} then the walker will in practice be bound to the node. This estimate is done by computing the correlation matrix, $C \equiv \langle x x^T \rangle$, and comparing $\langle x_1^2 \rangle^{1/2} = C_{11}^{1/2}$ with x_{1s}.

The linear correlation matrix can be computed as follows: form the outer product of Eq. (5) with its adjoint (neglecting the nonlinear term for this estimate) and take the ensemble average over the noise distribution. This leads to a dynamical equation for the correlation matrix: [$C(m) \equiv \langle x(m) x^T(m) \rangle$]:

$$C(m+1) = AC(m)A^T + \sigma_\eta^2 I. \tag{12}$$

Equation (12) is a linear dynamical system. Hence, if a stable fixed point exists, there is only one and it has a global basin of attraction. Equation (12) can be iterated, starting with $C(0)=0$, hence:

$$C(1) = \sigma_\eta^2; \quad C(2) = \sigma_\eta^2 (I + AA^T), \tag{13}$$

and so forth. It is straightforward to show that the fixed point, if it exists, is given by

$$C_* = \sigma_\eta^2 [I + AA^T + A^2 [A^T]^2 + \cdots + A^n [A^T]^n + \cdots]. \tag{14}$$

The fixed point C_* satisfies the equation

$$C_* = AC_* A^T + \sigma_\eta^2 I. \tag{15}$$

We now drop the * subscript for notational hygiene. A little algebra shows that the entries of the fixed point C satisfy

$$C_{jk} = \frac{1}{1-\lambda^2} [\lambda (C_{j,k+1} + C_{j+1,k}) + C_{j+1,k+1} + \sigma_\eta^2 \delta_{jk}] \tag{16}$$

for $j,k=1,2,\ldots,N$, with $C_{jk}=0$ understood for j or $k>N$. This should be viewed as an iteration scheme for the matrix entries of C where one starts with $j=k=N$ in the lower right hand corner and works to the upper left, making use of the fact that C is symmetric.

Now consider the asymptotic behavior as $\lambda\uparrow 1$. Using $1-\lambda=\epsilon$ [hence $1-\lambda^2=2\epsilon+O(\epsilon^2)$], and rewriting (16) to leading order in ϵ gives

$$C_{jk}\sim\frac{1}{2\epsilon}\left[C_{j,k+1}+C_{j+1,k}+C_{j+1,k+1}+\sigma_\eta^2\delta_{jk}\right]. \quad (17)$$

To leading order in ϵ, this implies

$$C_{jk}\sim\frac{\sigma_\eta^2}{2\epsilon}\left(\frac{1}{2\epsilon}\right)^{2N-(j+k)}\frac{[2N-(j+k)]!}{(N-j)!(N-k)!}\left[1+O(\epsilon)\right] \quad (18)$$

as can be shown by direct substitution. Defining $\beta\equiv 1/2\epsilon$ and $\gamma_{j+k}\equiv[2N-(j+k)]!/(N-j)!(N-k)!$, the correlation matrix can be written as

$$C\sim\frac{\sigma_\eta^2}{2\epsilon}\begin{pmatrix}\gamma_2\beta^{2N-2} & \gamma_3\beta^{2N-3} & \cdots & \\ \gamma_3\beta^{2N-3} & \ddots & & \beta^2 \\ & & 2\beta^2 & \beta \\ \cdots & \beta^2 & \beta & 1\end{pmatrix}. \quad (19)$$

From this it is possible to show that the largest eigenvalue of the correlation matrix C is asymptotically $\sim C_{11}$, i.e.,

$$\sigma_{x_1}^2\sim\sigma_\eta^2\gamma_2\left(\frac{1}{2\epsilon}\right)^{2N-1} \quad (20)$$

and its associated eigenvector points predominantly in the direction of x_1. Hence

$$\langle x_1^2\rangle^{1/2}\sim\sigma_\eta\gamma_2^{1/2}\left(\frac{1}{2\epsilon}\right)^{N-1/2}. \quad (21)$$

For the systems studied ($N=1,2,3,4$) the ratio $\gamma_2^{1/2}/2^{N-1/2}$ varies weakly, hence we choose a nominal value of $3/\sqrt{2}$. When dealing with larger N, however, this approximation should be done more carefully.

As mentioned before, $\langle x_1^2\rangle^{1/2}\sim x_{1s}$ is the regime where noise-driven escape begins to shut down. Taking this as our threshold for the noise amplitude leads to the following definition of $\sigma_{\min}$:

$$\sigma_{\min}(\epsilon;N)\equiv\frac{\sqrt{2}}{3}\,\epsilon^{2N-1/2}. \quad (22)$$

Figure 5 displays the results of a dozen different simulations using dimensions 1 through 4 and a wide range of noise scales. The escape time has been rescaled by the linear amplification time scale ($\tau'\equiv N\tau/\epsilon$) and the noise is rescaled by $\sigma_{\min}$ in each case [$\sigma'\equiv\sigma_\eta/\sigma_{\min}(\epsilon;N)$], which brings the noise-driven escape cutoff to $\sigma'\sim O(1)$. This figure shows several important things: (1) the high noise behavior is insensitive to ϵ but strongly dependent on dimensionality, (2) when the noise level reaches σ_c, the escape time begins to deviate strongly from the high noise behavior. The time scale

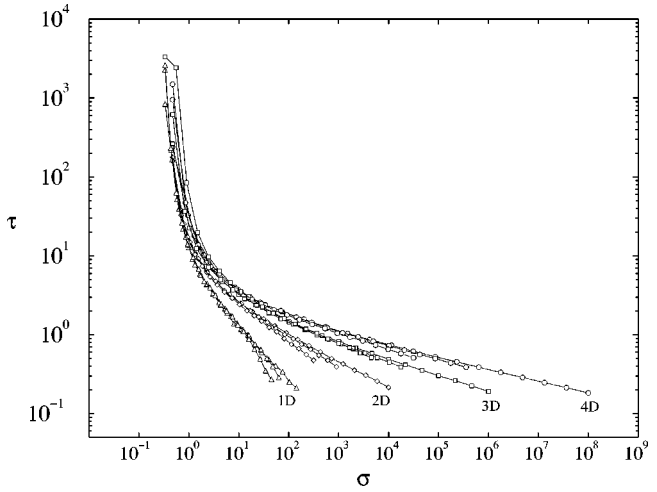

FIG. 5. A summary of twelve numerical runs, rescaled using the stretched time scale, $\tau'\equiv\epsilon\tau/N$, and noise scale $\sigma'\equiv(\sqrt{2}/3)\sigma/\epsilon^{2N-1/2}$. The motivation for these choices is given in the text. (The prime is not indicated on the axis labels due to limitations of the graphics routine.) The twelve different sets of data represent three values of the bifurcation parameter ($\epsilon=0.1$, 0.05, and 0.01) for $N=1$ through 4.

for escape in this noise range is $\sim N/\epsilon$, and (3) the noise cutoff for escape is well approximated by $\sigma_{\min}$.

It remains to derive the high noise scaling law (11). Consider the 2D case as an example. Returning to Eq. (5), now take the flow limit to convert this to a pair of ordinary differential equations (i.e., taking $I-A$ and b to be both $\sim\delta t$ the time step). We also focus only on the threshold behavior ($\epsilon=0$) for reasons stated previously. This gives

$$\begin{pmatrix}\dot{x}_1\\ \dot{x}_2\end{pmatrix}=\begin{pmatrix}0 & 1\\ 0 & 0\end{pmatrix}\begin{pmatrix}x_1\\ x_2\end{pmatrix}+\begin{pmatrix}0\\ x_1^2\end{pmatrix}. \quad (23)$$

Because this is a differential equation, the addition of noise is a subtle issue. We assume that a proper prescription is taken (e.g., the Stratonovich calculus). This leads to the following Fokker-Planck equation, which governs the evolution of the probability density, $f(x_1,x_2,t)$ [17]:

$$\frac{\partial f}{\partial t}=-x_2\frac{\partial f}{\partial x_1}-x_1^2\frac{\partial f}{\partial x_2}+D\left(\frac{\partial^2 f}{\partial x_1^2}+\frac{\partial^2 f}{\partial x_2^2}\right), \quad (24)$$

where the diffusion constant D is proportional to σ_η^2. In what follows, we assume this equation has already been nondimensionalized. Now introduce the rescalings:

$$\tau\equiv D^{\alpha_0}t;\quad \xi_j\equiv D^{\alpha_j}x_j,\quad j=1,2. \quad (25)$$

This takes Eq. (24) to (f_τ denotes $\partial f/\partial\tau$, etc.)

$$f_\tau=-D^a\xi_2 f_{\xi_1}-D^b\xi_1^2 f_{\xi_2}+D^c f_{\xi_1\xi_1}+D^d f_{\xi_2\xi_2}, \quad (26)$$

with $a=\alpha_1-\alpha_2-\alpha_0$, $b=\alpha_2-2\alpha_1-\alpha_0$, $c=1+2\alpha_1-\alpha_0$, and $d=1+2\alpha_2-\alpha_0$. The scaling exponents are chosen to make $a=b=c=0$, for reasons to be discussed below. This can be done if $\alpha_0=1/7$, $\alpha_1=-2/7$, and $\alpha_2=-3/7$, which forces $d=2/7$. Hence, in the $D\to 0$ limit Eq. (26) becomes

$$f_\tau = -\xi_2 f_{\xi_1} - \xi_1^2 f_{\xi_2} + f_{\xi_2\xi_2}. \tag{27}$$

The interpretation is as follows: in the low-noise limit at threshold ($\epsilon = 0$) the dominant effects experienced by a random walking particle are advection due to the deterministic flow, which is in essence a ''folded'' shear-type flow at the origin. (The interested reader is referred to Figure 7.3.1 of [3] for a diagram.) The advection is balanced by diffusion *only in the direction transverse to the stable manifold*, which is the x_2 direction near the origin, because the shearing motion develops sharp gradients only in the x_2 direction. The diffusion in the x_1 direction is negligible in comparison.

The fact that the scaling exponent $\alpha_0 = 1/7$ implies that the escape time should scale as $D^{-1/7} \sim \sigma_\eta^{-2/7}$.

In higher dimensions, a similar rescaling argument shows that the scaling exponents α_j obey the $N+1$ conditions

$$\alpha_{j+1} = \alpha_j - \alpha_0; \quad j = 1,2,\ldots,N-1;$$

$$\alpha_N = 2\alpha_1 + \alpha_0;$$

$$1 + 2\alpha_N - \alpha_0 = 0. \tag{28}$$

The first $N-1$ of these can be solved iteratively for α_1 and α_0 (i.e., $\alpha_2 = \alpha_1 - \alpha_0$; $\alpha_3 = \alpha_2 - \alpha_0 = \alpha_1 - 2\alpha_0$, etc.), leading to

$$\alpha_N = \alpha_1 - (N-1)\alpha_0. \tag{29}$$

This equation, in conjunction with the last two of Eq. (28), can now be solved easily, leading to $\alpha_0 = 1/(4N-1)$ and the scaling law (11). Notice that if, instead of the quadratic nonlinearity in Eq. (10), one had a cubic or some other subdominant behavior then the scaling exponents will change—albeit in a relatively simple manner.

Pressing on, one finds that $\alpha_j = -(N+j-1)/(4N-1)$ for $j = 1,2,\ldots,N$. The scale factors that appear in the diffusive terms of the N-dimensional Fokker-Planck equation, $D^{1+2\alpha_j-\alpha_0}$, have exponents $2(N-j)/(4N-1)$. Hence, all but the $j=N$ diffusive term vanish as $D \to 0$. This implies that the Fokker-Planck equation has a universal form in the zero-noise limit:

$$f_\tau = -\xi_2 f_{\xi_1} - \xi_3 f_{\xi_2} \cdots - \xi_1^2 f_{\xi_N} + f_{\xi_N\xi_N}. \tag{30}$$

That is, it involves all of the advective terms, but only the diffusive term associated with the direction that experiences the greatest linear amplification factor *below* threshold ($\epsilon > 0$).

V. BREAKING THE DEGENERACY

For the results of the preceding sections to be of physical interest they must survive breaking of the exact spectral degeneracy and uniformity of coupling assumed in Eq. (4). Once the exact degeneracy is broken the number of free parameters becomes large. The results reported here are only a preliminary study of this issue, as a full treatment is outside the scope of the paper as well as being an open area of investigation. Here, we focus on the four-dimensional case,

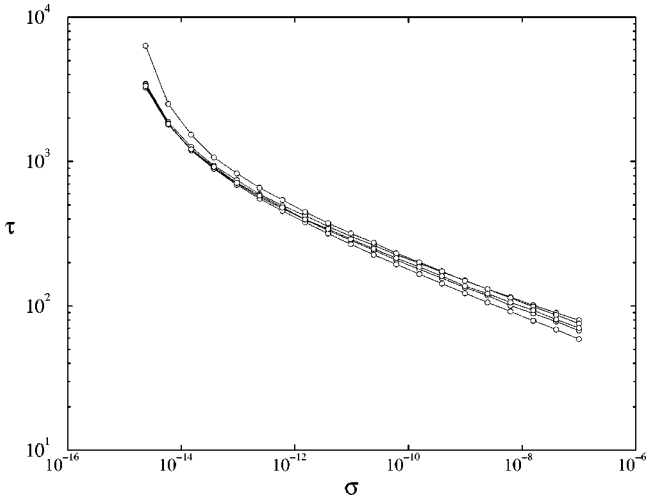

FIG. 6. The effect of variation of the off-diagonal coupling on noise-driven escape. The choice of off-diagonal terms is explained in the text.

as that should be the most fragile of the systems we have examined in this paper, and take the matrix A to be of the form

$$A \equiv \begin{pmatrix} \lambda_1 & a_{12} & a_{13} & a_{14} \\ 0 & \lambda_2 & a_{23} & a_{24} \\ 0 & 0 & \lambda_3 & a_{34} \\ 0 & 0 & 0 & \lambda_4 \end{pmatrix}. \tag{31}$$

All 4×4 matrices can be cast into upper triangular form by a unitary transformation [18], hence the form (31) is very general. We restrict attention to real entries, and keep off-diagonal terms positive (or zero) as the introduction of negative signs—especially in the terms immediately above the main diagonal—can change the bifurcation from subcritical to supercritical. All terms immediately above the main diagonal were kept nonzero and of order unity. The nonlinear term was unchanged.

First the dependence on the off-diagonal couplings was examined. In Fig. 6 the results of 5 different runs with $\epsilon = 0.01$ and various off-diagonal terms are shown (the diagonal terms are kept exactly degenerate and equal to $1-\epsilon = 0.99$). One set of data was generated using the original form of A for comparison (this is the data set that lies slightly above the others). Another was generated using all off-diagonal terms set to unity, while the other three had the off-diagonal terms chosen at random and order unity. Clearly, there is only a relatively weak dependence on the off-diagonal couplings as long as they remain positive and order unity and the diagonal terms are degenerate.

The effect of breaking the spectral degeneracy was considered next. The off-diagonal terms were reset to those of Eq. (4) and the eigenvalues were assigned the form $\lambda_j \equiv 1 - \epsilon\alpha_j$ for $j = 1,\ldots,4$. The values of α_j were chosen to be $\alpha_1 = 1$; $\alpha_2 = 0.1$; $\alpha_3 = 1$, and $\alpha_4 = 10$. (Notice they vary by 2 orders of magnitude.) As $\epsilon \downarrow 0$ we expect the scaling behavior to approach that of the threshold scaling for $N = 4$, as indeed happens. For larger values of ϵ, however, other scalings occur. This is also to be expected because breaking the spectral

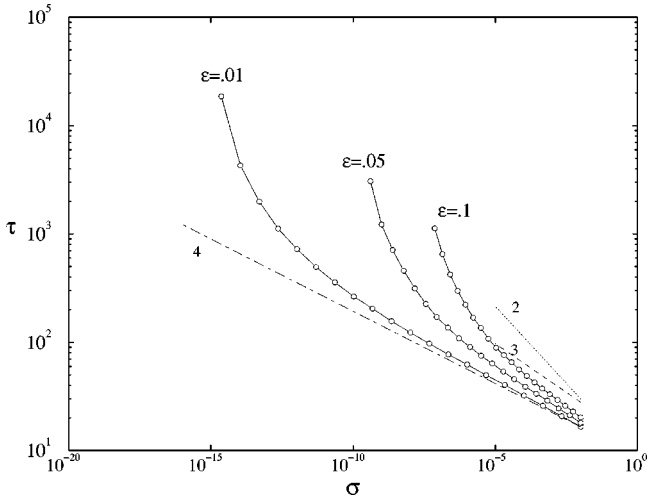

FIG. 7. The effect of breaking the spectral degeneracy. The form of the eigenvalues used is described in the text. Three values of ϵ are shown, as indicated. Also shown are the threshold scaling laws for $N=2$ (dotted line), $N=3$ (dashed line), and $N=4$ (dot-dashed line).

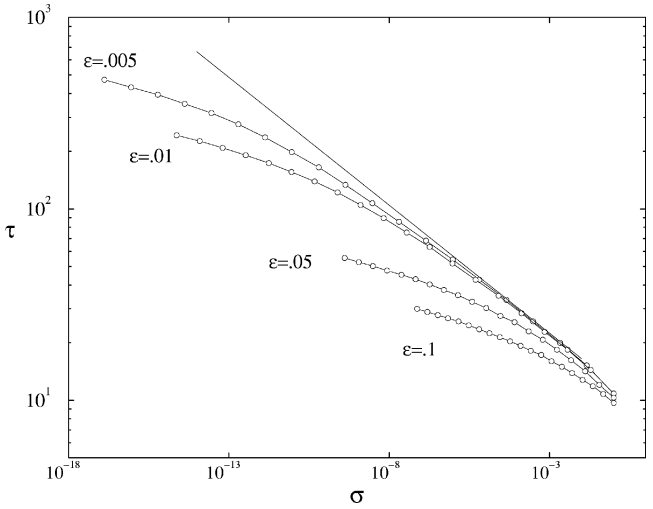

FIG. 8. The linearly unstable case. Here two of the eigenvalues are chosen to be unstable, and two are stable, hence the fixed point at the origin is now is a hyperbolic saddle.

degeneracy also destroys the geometric degeneracy. As the degeneracy is broken more strongly we would expect the scaling to be determined by the dimension of any remaining geometrically degenerate subspaces. A rough figure of merit for the present case is to compare the spread in eigenvalues,

$$\Delta\lambda \equiv \lambda_{\max} - \lambda_{\min}, \tag{32}$$

to their geometric mean,

$$\bar{\lambda} \equiv (\lambda_1\lambda_2\lambda_3\lambda_4)^{1/4}. \tag{33}$$

Now define

$$\gamma \equiv \frac{\Delta\lambda}{\bar{\lambda}}. \tag{34}$$

We expect that as $\gamma \to 0$ the system should behave as an N-dimensional degenerate system, while if γ is large it will deviate from this behavior.

In Fig. 7 the bifurcation parameter values $\epsilon=0.1$, 0.05, and 0.01 were used, giving $\gamma=0.1$, 0.6, and $+\infty$, respectively. (When $\epsilon=0.1$, $\lambda_4=0 \Rightarrow \bar{\lambda}=0$.) These results are compared with the threshold scaling laws for $N=2,3,4$. Clearly, for $\epsilon=0.01$ the system behaves essentially as though it were fourfold degenerate, while with $\epsilon=0.1$ it scales more like $N=2$ (λ_1 and λ_3 are still degenerate). At the intermediate value ($\epsilon=0.05$) the system arguably scales like $N=3$. Using only λ_1, λ_2, and λ_3 to compute γ gives $\gamma \approx 0.05$, which would imply that these three degrees of freedom are still degenerate.

Finally, we considered the linearly *unstable* case by setting $\lambda_2 = 1+\epsilon\alpha_2$ and $\lambda_4 = 1+\epsilon\alpha_4$ (all other entries were unchanged). This converts the node into a saddle. The numerical results are shown in Fig. 8. Notice that at high noise the scaling appears only slightly changed from the linearly stable case (the solid line is the $N=4$ threshold scaling). At low noise the random walkers escape much faster than their linearly stable counterparts, as expected.

VI. SUMMARY

In summary, we have shown that Takens-Bogdanov equilibria have noise response characteristics that are distinct from normal systems that have diagonalizable linear terms. In particular, the escape time at high noise levels obeys the scaling law (11) with the exponent $\nu_N = 2/(4N-1)$, depending only on the dimension of the subspace exhibiting geometric degeneracy. A preliminary study shows that these scaling characteristics are relatively robust under weak breaking of the degeneracy. Statistical robustness, in spite of topological fragility, suggests that the nongeneric aspects of the bifurcation are less restrictive than previously thought. Hence, these effects might be observable in experimental situations.

Note added in proof. After this paper was accepted for publication, the authors became aware of related work by Manneville [19]. The authors thank Dr. Manneville for pointing out this reference.

ACKNOWLEDGMENTS

E.R.T. would like to thank K. Lindenberg and G. Weiss for helpful and encouraging comments. X.Z.T. would also like to acknowledge the hospitality of the Applied Physics Department of Columbia University. This work was supported by the U.S. AFOSR and DOE. C.K. was supported by the NSF Research Experience for Undergraduates program at W&M.

[1] F. Takens, Publ. Math. IHES **43**, 47 (1974).
[2] R. I. Bogdanov, Funct. Anal. Appl. **9**, 144 (1975).
[3] J. Guckenheimer and P. Holmes, *Nonlinear Oscillations, Dynamical Systems and Bifurcations of Vector Fields* (Springer-Verlag, New York, 1993).
[4] L. N. Trefethen, A. E. Trefethen, S. C. Reddy, and T. A. Driscoll, Science **261**, 578 (1993).
[5] B. F. Farrell and P. J. Ioannou, Phys. Rev. Lett. **72**, 1188 (1994).
[6] B. F. Farrell and P. J. Ioannou, Phys. Fluids A **8**, 1257 (1996).
[7] J. S. Baggett and L. N. Trefethen, Phys. Fluids A **9**, 1043 (1997).
[8] T. Gephardt and S. Grossman, Phys. Rev. E **50**, 3705 (1994).
[9] P. J. Holmes, Physica D **2**, 449 (1981).
[10] F. E. McCaughan, SIAM J. Appl. Math. **50**, 1232 (1990).
[11] J. D. Crawford and E. Knobloch, Physica D **31**, 1 (1988).
[12] I. M. Moroz and S. Leibovich, Phys. Fluids **28**, 2050 (1985).
[13] T. Sauer, C. Grebogi, and J. A. Yorke, Phys. Rev. Lett. **79**, 59 (1997).
[14] K. Lindenberg and G. Weiss (private communication).
[15] L. Jaeger and H. Kanz, Physica D **105**, 79 (1997).
[16] E. R. Tracy and X.-Z. Tang, preprint available at http://xxx.lanl.gov/abs/physics/9802053
[17] K. Lindenberg, B. West, and J. Masoliver, in *Noise in Nonlinear Dynamical Systems*, edited by F. Moss and P. V. E. McClintock (Cambridge, New York, 1989).
[18] G. H. Golub and C. F. van Loan, *Matrix Computations*, 2nd ed. (Johns Hopkins University Press, Baltimore, 1991).
[19] P. Manneville, J. Phys. II **7**, 371 (1997).